Pure Appl. Chem., Vol. 80, No. 8, pp. 1651–1668, 2008.
doi:10.1351/pac200880081651

Diverse approaches to the controlled generation of nanotextured surfaces*

Jeremy J. Ramsden‡

Department of Materials, Cranfield University, Bedfordshire MK43 0AL, UK

Abstract: Smooth, chemically uniform surfaces are seldom found in nature. Mimicry of natural variegation is a powerful approach for controlling chemical affinity at the nanoscale. Molecular recognition is one of the fundamental concepts underlying the functioning of living cells, and it depends on a particular relationship between the nanoscale, i.e., molecular, variegations of two potentially interacting molecular partners. The primary subject matter of this paper is how to artificially generate appropriate nanoscale texture at the surfaces of materials. Excluding "pick and place" chemistry, in which essentially a Maxwellian demon intervenes to place objects with atomic precision, and nowadays achievable through an adaptation of atomic force microscopy, on the grounds that it is too slow to be practicable for fabricating useful quantities of material, three approaches are explored in some detail: (i) "powder", i.e., mixing at least two individually monofunctional (with respect to the ultimate molecular recognition task) precursor components (possibly with secondary functionality enabling them to appropriately self-assemble on a substratum); (ii) mixing polymers with the possibility of phase separation and frustrated phase separation with block copolymers; and (iii) felting. The emphasis is on processes that create more or less irregular structures, rather than regular arrays. The final section deals with the metrology of nanotexture.

Keywords: morphology; chemical variegation; pick and place; powder mixing; polymer mixing; phase separation; block copolymers; felting.

INTRODUCTION

Smooth, chemically uniform surfaces are seldom found in nature. On the contrary, variegation is found over a huge variety of length scales, such as the camouflaging spots and other patterns in the fur coats or scales of animals (Fig. 1) and the intricate textures of metamorphic rocks visible to the naked eye, down to the fantastic variety of lipid molecules found in the outer membranes of living cells [1] and the surfaces of proteins [2], visible only with the aid of powerful magnifying instruments such as various kinds of microscopes. The last named examples are of particular relevance here because they are actual examples of truly nanotextured surfaces.

*Paper based on a presentation at the 41st IUPAC World Chemistry Congress, 5–11 August 2007, Turin, Italy. Other presentations are published in this issue, pp. 1631–1772.

‡Tel.: +44 1234 754100; Fax: +44 1234 751346; E-mail: j.ramsden@cranfield.ac.uk

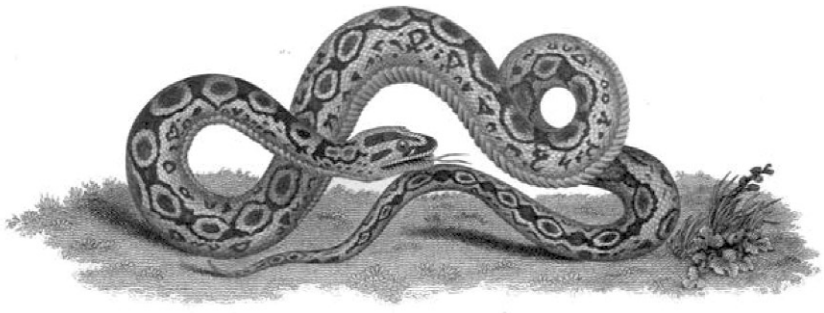

Fig. 1 Boa constrictor [3].

Here I distinguish between nanopattern and nanotexture. The former term refers to regular arrangements, and the latter to irregular ones. There is of course no absolute distinction between the two [4,5]. It is always difficult to be certain of the absence of any regularity, although for a finite object that is not too large, exhaustive enumeration may, in principle, provide certainty. As a provisional working statement, I suggest defining pattern as "a regularity that can be perceived by human vision within a few seconds of observation".[1]

"Observation" here also includes the help, very necessary at the nanoscale, of delicate instruments such as scanning probe microscopes (SPMs).[2] Texture then covers irregularity, ranging from the point where regularity is no longer (almost) immediately perceptible, to complete randomness. We shall return to the question of how to quantify irregularity in the section "Analysis of texture".

Given the intricately regulated web of protein interactions inside any living cell [6,7], it can hardly be expected that the arrangement of chemical functionalities on the surface of a protein is really random, even though at first glance it appears to be. On the contrary, it may be presumed that it has evolved to satisfy requirements, stringent and subtle at the same time, for interacting with other biopolymers to greater or lesser extents.[3] Such interactions are fundamental to the maintenance of life. I propose (although this paper will not deal with testing the proposition) that natural nanotextures for the purposes of recognition maximize the complexity of the surface arrangements.

Similar considerations apply to the interactions between cells in metazoans (multicellular organisms), especially when the single cell from which all organisms start differentiates into different types of cells. The cell is about three orders of magnitude larger than a protein, and the nanotexture of cell surfaces does not seem to be due to particular arrangements of functionally different lipid head groups in exact equivalence to the arrangements of functionally different amino acid residues on the surface of a protein, but rather to rafts of functionally similar lipids grouped together, and to the arrangement of the numerous protein molecules (that typically cover about half of the surface of a eucaryotic cell) embedded in the cell membrane [9]. Note that this texture is still within the range that is normally considered to comprise the nanoscale [10]. Recent advances in imaging technology have also revealed a dynamic morphological structure on the surfaces of living cells [11].

[1]Preconditioning the data is not precluded, e.g., by associating each point with some metric, possibly followed by principal component analysis or the like to reduce the dimensionality, and then looking for clusters.

[2]It is of course important that the data processing used to create the image presented to the human eye should avoid superimposing any kind of preconceived regularity on the image, as is sometimes done via Fourier transforms and averaging to increase effective resolution by increasing the signal:noise ratio of the image.

[3]In these interactions, the concept of the dehydron [8] plays a particularly important role. Protein–protein recognition is in fact now reasonably well understood, although there is still a large element of heuristics in the modeling approaches used to design artificial receptors. Hence, one can at least say that it is reasonably well understood in principle, although those principles have not yet all been translated into practical algorithms for design.

Molecular recognition may be considered to be one of the fundamental processes underlying the phenomenon of life, especially its regulatory (and hence adaptive) aspects. While nanotexture undoubtedly occurs in purely inanimate systems, the overwhelming bulk of examples of functional nanotexture occurs in the living world; indeed, my particular interest in the topic lies in its relevance to the interface between the living and the nonliving worlds.

ONE-DIMENSIONAL TEXTURE

Preliminary to the discussion of nanotexture proper, which implies a two-dimensional arrangement of features important for molecular and cellular recognition, let us consider the one-dimensional situation, which is of course much simpler. The purpose of this section is to look at some relatively straightforward parameters that might be used as means to quantify texture. A one-dimensional sequence of symbols (each symbol representing a topographical feature, such as a height, or a chemical element in a particular oxidation state) can be completely defined by the set of probability distributions $W_1\,(yx)\mathrm{d}y$, the probability of finding y, the value of the symbol, in the range $(y, y + \mathrm{d}y)$ at position x (if one is moving along the sequence at a uniform rate, this might be equivalent to a time t), $W_2(y_1x_1, y_2x_2)\mathrm{d}y_1\mathrm{d}y_2$, the joint probability of finding y in the range $(y_1, y_1 + \mathrm{d}y_1)$ at position x_1 and in the range $(y_2, y_2 + \mathrm{d}y_2)$ at position x_2, and so on for triplets, quadruplets, and higher multiples of values of y. If there is an unchanging underlying mechanism generating the sequence, the probabilities are stationary and the distributions can be simplified as $W_1(y)\mathrm{d}y$, the probability of finding y in the range $(y, y + \mathrm{d}y)$; $W_2(y_1y_2x)\mathrm{d}y_1\mathrm{d}y_2$, the joint probability of finding y in the ranges $(y_1, y_1 + \mathrm{d}y_1)$ and $(y_2, y_2 + \mathrm{d}y_2)$ when separated by an interval $x = x_2 - x_1$; etc. If successive values of y are not correlated at all, i.e.,

$$W_2(y_1x_1, y_2x_2) = W_1(y_1x_1)\; W_1(y_2x_2) \tag{1}$$

etc., all information about the process is completely contained in W_1, and the process is called a purely random process. If, however, the next step of a process depends on its current state, i.e.,

$$W_2(y_1y_2x) = W_1(y_1)\; P_2(y_2|y_1x) \tag{2}$$

where P_2 denotes the conditional probability that y is in the range $(y_2, y_2 + \mathrm{d}y_2)$ after having been at y_1 at an earlier position x, we have a Markov chain, defined as a sequence of "trials" (that is, events in which a symbol can be chosen) with possible outcomes **a** (possible states of the system), an initial probability distribution $\mathbf{a}^{(0)}$, and (stationary) transition probabilities defined by a stochastic matrix P [12].[4] The probability distribution for an r-step process is

$$\mathbf{a}^{(r)} = \mathbf{a}^{(0)}\; P^r \tag{3}$$

The Markov transition matrix, if it exists, is a compact way of representing texture.

If upon repeated application of P the distribution **a** tends to an unchanging limit (i.e., an equilibrial set of states) that does not depend on the initial state, the Markov chain is said to be ergodic, and

$$\lim_{r\to\infty} P^r = Q \tag{4}$$

where Q is a matrix with identical rows. Now

$$PP^n = P^nP = P^{n+1} \tag{5}$$

[4]The random walk is an example of a Markov chain. A random sequence, i.e., with a total absence of correlations between successive symbols, is a zeroth order Markov chain. Without loss of generality, we can consider a binary string, which is a linear sequence of zeros and ones, and, again without loss of generality, we can consider that the overall frequencies of occurrence of the two symbols are equal. Such sequences can be generated by choosing successive symbols with probability $p = 0.5$.

and if Q exists it follows, by letting $n \to \infty$, that

$$PQ = QP = Q \tag{6}$$

from which Q (giving the stationary probabilities, i.e., the equilibrial distribution of **a**) can be found. Note that if all the transitions of a Markov chain are equally probable, then there is a complete absence of constraint, in other words, the process is purely random.

The entropy of a Markov process is the "average of an average" (i.e., the weighted variety of the transitions). For each row of the stochastic matrix, an entropy $H = -\sum_i p_i \log_2 p_i$ (Shannon's formula) is computed. The (informational) entropy of the process as a whole is then the average of these entropies, weighted by the equilibrial distribution of the states.

Another approach to characterize texture is to make use of the concept of a run, defined as a succession of similar events preceded and succeeded by different events. Let there again be just two kinds of elements, 0 and 1, and let there be n_0 0s and n_1 1s, with $n_0 + n_1 = n$. r_{0i} will denote the number of runs of 0 of length i, with $\sum_i r_{0i} = r_0$, etc. It follows that $\sum_i r_{0i} = n_0$, etc. Given a set of 0s and 1s, the numbers of different arrangements of the runs of 0 and 1 are given by multinomial coefficients and the total number of ways of obtaining the set $r_{ji}(j = 1, 2; i = 1, 2, \ldots, n_0)$ is [13]

$$N(r_{ji}) = \begin{bmatrix} r_0 \\ \\ r_{0i} \end{bmatrix} \begin{bmatrix} r_1 \\ \\ r_{1i} \end{bmatrix} F(r_0, r_1) \tag{7}$$

where the terms denoted with square brackets are the multinomial coefficients, which give the number of ways in which n elements can be partitioned into k subpopulations, the first containing r_0 elements, the second r_1, etc.:

$$\begin{bmatrix} r \\ \\ r_i \end{bmatrix} = \frac{n!}{r_0!\, r_1 \ldots r_k!}, \text{ with } \sum_i^{i=k} r_i = n \tag{8}$$

and the special function $F(r_0, r_1)$ is the number of ways of arranging r_0 objects of one kind and r_1 objects of another so that no two adjacent objects are of the same kind (see Table 1). Since there are $\binom{n}{n_0}$ possible arrangements of the 0s and 1s, the distribution of the r_{ji} is

$$P(r_{ji}) = \frac{N(r_{ji}) F(r_0, r_i)}{\binom{n}{n_0}} \tag{9}$$

The deviation of the actually observed distribution from eq. 9 can be used as a statistical parameter of texture.

Table 1 Values of the special function $F(r_0, r_1)$.

$\lvert r_0 - r_1 \rvert$	$F(r_0, r_1)$
>1	0
1	1
0	2

One very important physical instantiation of one-dimensional texture is the sequences of nucleic acids that encode proteins and also constitute the binding sites (promoters) for transcription factors—proteins that bind to DNA as a prerequisite for the transcription of the DNA into RNA that precedes the translation of the RNA into amino acid sequences (proteins) [14]. The nucleic acids have a variety of four (the bases A,U,C,G in natural RNA, and A,T,C,G in DNA). Many statistical investigations of intragenome DNA correlations group the four into purines (A and G) and pyrimidines (U or T and C)—rather like analyzing texts (Markov himself converted the poems of Pushkin into sequences of vowels and consonants for analysis [15]).

HOW TO GENERATE NANOSCALE TEXTURE IN MATERIALS

The use of SPMs to characterize structure at the nanoscale suggests the reciprocal use of SPM-based methods to generate such structure, that is, by picking up atoms from a store and placing them exactly where required, as was first proposed by Drexler [16]. The embracing of such a eutactic environment, with every atom placed in a precise location, is not perhaps the best way to achieve the types of structures described in the Introduction, however. Firstly, there is the problem of throughput. Although an early example, the assembly of xenon atoms spelling out the letters "IBM" [17] achieved almost iconic status, the extreme laboriousness of the procedure made it an impracticable tour de force.[5] Even subsequent developments such as the IBM "Millipede" project [20], in which large numbers of SPM tips work in parallel, still fall many orders of magnitude short of the throughput that would be required for materials fabrication. Secondly, until now at any rate, the procedure is extremely limited with regard to possible choices of atoms. Drexler himself has focused on diamondoid (carbon) structures [21], but in the natural examples of nanotextured surfaces, the variegation tends to be provided as much or more by chemical variety than by morphology. Thirdly, the natural examples appear to be characterized by statistical (ir)regularity (although this must be considered as only a provisional statement), which might well be mimicked by self-assembly process offering much higher throughput than Drexlerian mechanosynthesis. In the remainder of this paper, therefore, I shall focus on chemical rather than mechanical ways of achieving nanotexture.[6]

As well as the mimicry of natural surfaces for biological molecular recognition, the fabrication techniques to be described should be generally applicable to create feature sizes in the nanometer range (i.e., 1–100 nm), which is still difficult to achieve using conventional top-down semiconductor processing techniques [24]. Furthermore, self-assembly is more flexible regarding the geometry of the substratum to which it can be applied, e.g., there is no restriction to planar surfaces. This is particularly advantageous if it is desired to engineer the surfaces of intricately curved objects such as vascular stents in order to increase their biocompatibility [25].

The next three sections will deal in turn with three diverse ways of generating statistical texture: (i) "powder", i.e., mixing at least two essentially monofunctional (with respect to the ultimate molecular recognition task) precursor components (possibly with secondary functionality enabling them to appropriately self-assemble on a substratum); (ii) mixing polymers, with the possibility of phase separation, and frustrated phase separation using block copolymers (dealt with rather cursorily in this paper, since nanotextured block copolymer-based thin films are the topic of a forthcoming article [J. J. Ramsden, in preparation]); and (iii) felting. Textures generated by reaction-diffusion processes (Turing

[5]A similar comment applies to subsequent demonstrations of "pick and place" chemistry [18,19].

[6]At a length scale slightly larger than that of atoms, dip pen nanolithography has been developed by Mirkin as a way of placing molecules in finely resolved zones of a substratum [22,23]. The technique works by coating the SPM tip with a weakly adherent molecular ink (e.g., proteins, relatively weakly adhering to a hydrophilic tip). When it is desired to write, the tip is lowered to the vicinity of the substratum, to which the affinity of the ink is much stronger, and the ink's molecules are transferred to the substratum through a water meniscus (it follows that writing is strongly dependent on the ambient relative humidity).

patterns) are not covered, since until now it is not been possible to use them to generate nanotexture (nevertheless, as is well known, they are considered to be the mechanism of morphogenesis in biology (e.g., Fig. 1), suggesting that there might be some, as yet uncharacterized, nanoscale precursor of the larger-scale, readily visible structures that are the endpoint of these processes).[7]

PARTICLE SELF-ASSEMBLY

The paradigm for this process is the shaking and stirring of a powder—a collection of small (with respect to the characteristic length scale of the final texture) particles initially randomly mixed up. I consider a binary mixture of type A and B particles, supposing that no new principles emerge from more highly variegated mixtures. The interaction energy v is given by the well-known Bragg–Williams expression

$$v = v_{AA} + v_{BB} - 2v_{AB} \tag{10}$$

where the three terms on the right are the interaction energies (enthalpies) for A with itself, B with itself, and A with B. Naïvely, one would say that the mixture is miscible if $v < 0$, and immiscible otherwise. If the interaction energies are all zero, there will still be an entropic drive toward mixing (the case of the perfect solution). Edwards and Oakeshott [27] introduce the compactivity X, analogous to the temperature in thermodynamics, defined as

$$X = \partial V/\partial S \tag{11}$$

where V is the volume and S the entropy, defined in analogy to Boltzmann's equation as $S = \lambda \ln \Omega$, where Ω is the number of configurations. If the number of particles of type A at a certain point r_i is $m_A^{(i)}$ (equal to either zero or one), and since necessarily $m_A^{(i)} + m_B^{(i)} = 1$, by introducing the new variable $m_i = 2m_A^{(i)} - 1 = 1 - 2m_B^{(i)}$, we have $m_i = \pm 1$. Defining $\phi = \langle m_i \rangle = \tanh \varepsilon\phi/\lambda X$, three régimes are identified depending on the interaction parameter [27]:

- miscible: $v/\lambda X < 1$, $\phi = 0$;
- domains of unequal concentrations: $v/\lambda X > 1$, ϕ small;[8]
- domains of pure A and pure B: $v/\lambda X \gg 1$, $\phi = \pm 1$.

Considering a monolayer of particles on the substratum, if the mixed components are electrostatically charged, and at least one of them is mobile, a phase-separated (patchy) structure can occur in equilibrium [28].

Experimental results using particle assembly

Remarkably little effort seems to have been made to verify the theory described in the preceding section. In principle, the approach of assembling particles could be carried out either at the solid/liquid (e.g., [29]) or at the liquid/air (e.g., [30]) interfaces, but this does not appear to have been attempted with particle mixtures. One possible approach is to achieve potentially highly selective particle-particle binding by coating nanoparticles with oligonucleotides (cf. the section "One-dimensional texture") (sequences and their complementary sequences). The technology for doing this has been developed in the context of decorating selected DNA sequences using complementary DNA-coated microparticles (e.g., [31]).

[7]Such processes can be observed microscopically in, for example, embryonic insects and have been modeled accordingly [26].
[8]$X = v/\lambda$ emerges as a kind of critical point.

If two different immiscible amphiphiles are mixed on the Langmuir trough, the resulting variegated structures can be imaged using SPM after transferring the Langmuir film to a solid support using the Langmuir–Blodgett technique (Fig. 2). These experiments [32] have shown (a) how difficult it is to find convenient mixtures and (b) how difficult it is to predict theoretically what patterns result. There are moreover experimental difficulties in imaging texture (see the section "Visualizing and converting nanotexture) at scales below a few tens of nanometers. The lack of metrology techniques suited for this purpose is in fact one of the main current hindrances to progress in the field.

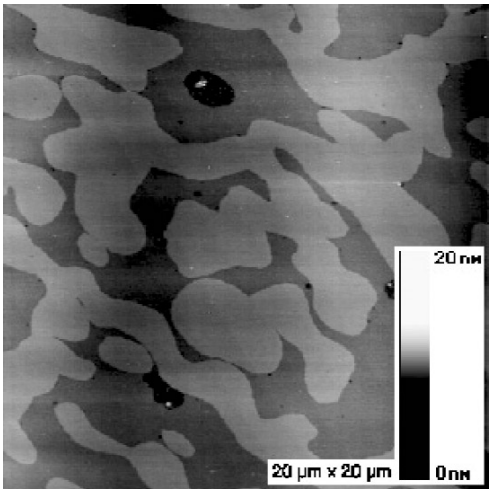

Fig. 2 Scanning force micrograph (contact mode) of a mixed behenic acid/pentadecanoic acid film transferred horizontally onto muscovite mica at a surface pressure of 15 mN/m. Image size: 20 × 20 µm [32] (reprinted with permission from Collegium Basilea).

Nanostructures assembled from a single type of particle

Competing interactions

Weakly electrostatically charged quantum dots (nanoparticles) suspended in water aggregate to form uniformly sized superspheres containing several hundred nanoparticles [33]. Nearest neighbors interact with weak, short-range van der Waals interactions, which easily dominate the slight electrostatic repulsion between them. Because, however, the electrostatic interaction is long-range (it can be tuned by varying the ionic strength of the solution), the overall electrostatic repulsion within a supersphere gradually accumulates, and when a certain number of nanoparticles have been aggregated, the electrostatic repulsion exceeds the attractive van der Waals force between nearest neighbors [34]. To form superspheres, the attractive interaction should be short-range, and the repulsive interaction should be long-range.

Mismatched epitaxy

We should first recall some facts about wetting.[9] An interface may be characterized by a surface or interfacial tension, i.e., free energy per unit area, usually denoted γ. A droplet of a liquid L on the solid

[9]The term "wetting" is used regardless of the nature of the liquid. Hence, "dry" here means not that water is absent, but that all liquid is absent.

S, in an environment of vapor V, forms a contact angle θ with the surface and according to Young's law:

$$\gamma_{LV} \cos \theta = \gamma_{SV} - \gamma_{SL} \tag{12}$$

which follows from the condition that at equilibrium the energies must be invariant with respect to small shifts dx of the position of the triple line T, where the three phases meet. Complete wetting is characterized by $\theta = 0$, implying (from eq. 12)

$$\gamma_{LV} = \gamma_{SV} - \gamma_{SL} \tag{13}$$

Cooper and Nuttall defined a spreading coefficient S as [35]:

$$S = \gamma_{\tilde{S}V} - \gamma_{SL} - \gamma_{LV} \tag{14}$$

where $\gamma_{\tilde{S}V}$ is the interfacial tension of a dry solid. Three régimes of S can be identified:

1. $S > 0$, corresponding to $\gamma_{\tilde{S}V} > \gamma_{SV}$, i.e., the wetted surface has a lower energy than the unwetted one, and wetting takes place spontaneously. The thickness h of the film is greater than monomolecular if $S \ll \gamma_{LV}$. The difference $\gamma_{\tilde{S}V} - \gamma_{SV}$ can be as much as 300 mJ/m^2 for water on metal oxides. Such systems therefore show enormous hysteresis between advancing and receding contact angles.[10]
2. $S = 0$. Occurs if $\gamma_{\tilde{S}V}$ practically equals γ_{SV}, as is typically the case for organic liquids on molecular solids.
3. $S < 0$. Partial wetting. Films thinner than a certain critical value, usually ~1 mm, break up spontaneously into droplets.

Explicitly considering the epitaxial growth of semiconductors, when material B is evaporated onto a substrate of a different material A, three analogous situations can arise:

- Frank–van der Merwe (B wets A, and a uniform layer is formed);
- Volmer–Weber (no wetting, hence, islets distributed in size of B on A are formed);
- Stranski–Krastanov (B can wet A, but there is a slight lattice mismatch between A and B, and the accumulating strain energy is ultimately sufficient to cause spontaneous dewetting, resulting in the formation of rather uniform islets of B, which relieves the strain[11]).

Miscellaneous processes

Physical and chemical vapor deposition processes are often able to yield structure at the nanoscale, or the lower end of the microscale, with some structural control achievable via the deposition parameters. An example is described by Ortmann et al. [37]. The structures obtained emerge from a particular combination of deposition parameters and must be established experimentally. Theoretical understanding of the structure and process is still very rudimentary, although attempts are under way (such as the "structure zone model", e.g., [38]).

Electrostatic spray deposition (ESD)

Ceramic precursors are dissolved in a suitable solvent and mixed immediately prior to forcing through an orifice maintained at a high potential difference with respect to the substratum. The liquid breaks up into electrostatically charged droplets, which are attracted both by gravity and the Coulombic force to the substratum, which is typically heated to accelerate the reaction that forms the final material. For example, calcium nitrate and phosphoric acid dissolved in butyl carbitol and atomized upon leaving the nozzle at a potential of 6–7 kV with respect to a titanium or silicon substratum maintained at a few hun-

[10]Other sources of hysteresis include chemical and morphological inhomogeneity (contamination and roughness) [36].
[11]There is still much discussion regarding the exact mechanism.

dred °C about 30 mm below the nozzle create coatings of calcium phosphate with intricate and intriguing nanostructures [39].

MIXED POLYMERS

The free energy M of mixing two polymers A and B is

$$M = \phi_A \ln \phi_A/N_A + \phi_B \ln \phi_B/N_B + \chi\phi_A\phi_B \quad (15)$$

where N_B and N_B are the degrees of polymerization, and χ is the Flory interaction parameter. The first two terms on the right-hand side of eq. 15, corresponding to the entropy of mixing, are very small due to the large denominators, hence the free energy is dominated by the third term, giving the interaction energy. If $\chi > 0$, then phase separation is inevitable. For a well-mixed blend, however, the separation may take place exceedingly slowly on laboratory timescales, and therefore for some purposes nanotexture might be achievable by blending two immiscible polymers. However, even if such a blend is kinetically stable in the bulk, when prepared as a thin film on the surface, effects such as spinodal decomposition may be favored due to the symmetry-breaking effect of the surface (e.g., by attracting either A or B). Solvent can have a marked effect on the morphology of the demixed films [40].

Block copolymers

As noted above, one of the problems with mixing weakly interacting particles of two or more different varieties is that under nearly all conditions complete segregation occurs, at least if the system is allowed to reach equilibrium. This segregation is, however, frustrated if the different varieties are covalently linked together, as in a block copolymer. A rich variety of nanotexture results from this procedure. If A and B, assumed to be immiscible ($\chi > 0$) are copolymerized to form a molecule of the type AAA···AAABBB···BBB (a diblock copolymer), then of course the A and B phases cannot separate in the bulk, hence microseparation results, with the formation of domains with size ℓ of the order of the block sizes (that is, at the nanoscale), minimizing the interfacial energy between the incompatible A and B regions. One could say that the entropy gain arising from diminishing the A–B contacts exceeds the entropic penalty of demixing (and stretching the otherwise random coils at the phase boundaries). The block copolymer can also be thought of as a type of supersphere [34]. If χN is fairly small (less than 10) we are in the weak segregation régime and the blocks tend to mix; but in the strong segregation régime (at $\chi N \gg 10$, the microdomains are almost pure and have narrow interfaces). As the volume fraction of one of the components (e.g., A) of the commonly encountered coil-coil diblock copolymers increases from 0 to 1, the bulk morphologies pass through a well-characterized sequence of body-centered cubic spheres of A in B, hexagonally packed cylinders of A in B, a bicontinuous cubic phase of A in a continuous matrix of B, a lamellar phase, a bicontinuous cubic phase of B in a continuous matrix of A, hexagonally packed cylinders of B in A, and body-centered cubic spheres of B in A [41–43].

When block copolymers are prepared as thin films (thickness d less than 100 nm) on a substratum (e.g., by spin- or dip-coating), the symmetry of the bulk system is broken, especially if one of the blocks of the copolymer is preferentially attracted to or repelled from the surface of the substratum [44].

If $d < \ell$, the surface may be considered to have a strong effect on the structure of the thin film. For example, poly-2-vinylpyridine does not wet mica, and a polystyrene-polyvinylpyridine block copolymer thin film on mica has a structure different from that of the copolymer in the bulk [45]: structures such as antisymmetric surface-parallel lamellae, antisymmetric hybrid structures (cf. Stranski–Krastanow film growth, the section "Mismatched epitaxy"), and surface-perpendicular lamellae or columns are typically formed. There is at present considerable interest in such processes for fabricating photolithography masks in the nanoscale range more conveniently than by electron beam writing. Reticulated structures seem to have been investigated the most extensively: block copolymer micelles can be formed by dissolving the polymer in a fluid that is a solvent for only one of the com-

ponents, and then used to coat surfaces, yielding a more or less regular array. This process has attracted interest as a route to making nanoporous membranes. For example, polystyrene-polymethylmethacrylate (PMMA) copolymers prepared with the volume fraction such that there are cylindrical microdomains of the PMMA in the bulk, can be coated on a suitable substratum (silicon or silica) such that the cylinders are oriented normal to the surface. Exposure to UV light cross-links the polystyrene but degrades the PMMA, which can then be selectively dissolved out of the film, leaving a nanoporous polystyrene membrane with pore size controllable by varying the molecular weight of the copolymer [46].

One advantage of these polymer-based processes is the tremendous variety of starting materials available (by the same token, the systematic experimental investigation of the effects of compositional variation across the whole range of possibilities represents a huge undertaking). As well as changing the chemical nature of the monomers and the degrees of polymerization, the block copolymers have also been mixed with homopolymers as a way of modifying the characteristic scale of the texture [47].

FELTING

The fabrication of texture by felting has been known for centuries (in Europe and much longer in China) in the guise of papermaking [48].[12] Paper is a thin sheet material made from vegetable fibers (typically based on cellulose) felted together. The fibers are macerated until each individual filament is a separate unit, mixed with water, and lifted from it in the form of a thin layer by the use of a sieve-like screen, the water draining through its small openings to leave a sheet of matted fiber upon the screen's surface. The first papermaking machine was invented by Robert in France at around the end of the 18th century, and was later perfected by two Englishmen, the Fourdrinier brothers. The machine poured the fibers out in a stream of water onto a long wire screen looped over rollers; as the screen moved slowly over the rollers, the water drained off and delivered an endless sheet of wet paper.

With the advent of various kinds of nanofibers, it is now possible to make paper-like materials at the nanoscale. This has been attempted most notably using carbon nanotubes (CNTs) [49,50], when it is sometimes called buckypaper. The process is different from the shaking and/or stirring used to prepare a mixed powder. Randomly oriented fibers (highly elongated objects) are rapidly placed on top of each other, with their long axes parallel to a substratum (which is, in the case of cellulose-based handwriting paper, removed later on) to form a random fiber network (RFN). The network coheres because of numerous fiber–fiber contacts, but the structure is different from that formed by the entanglement of very long polymers (cf. [51]). The deposition of fibrous proteins such as laminin in the presence of divalent cations as such as calcium allows sheets of arbitrary thickness to be assembled [52]. These structures mimic the basement membranes (extracellular matrix) that act as substrata for cells in living organisms. Mixtures of fibers would be especially interesting for creating nanotexture.

Simplified models, such as the RFN, into which the only input is the actual distribution of fiber lengths and their surface chemical properties, are useful for calculating basic properties of felted materials, for example, mass distribution, number of crossings per fiber, fractional contact area, free-fiber length distribution, and void structure (e.g., [53,54]).

[12]Papermaking is reputed to have been invented in A.D. 105 by Ts'ai Lun in China. It arrived in Europe, firstly in Italy, by the end of the 13th century, probably via Samarkand, Baghdad, Damascus, Egypt, the Maghreb, and Muslim Spain (it appeared in England around 1490).

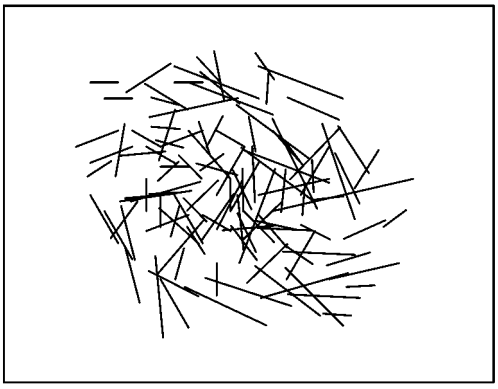

Fig. 3 Sketch of a two-dimensional RFN used to model a felted assembly.

VISUALIZING AND CONVERTING NANOTEXTURE

A significant challenge in the field is the metrology of fabricated surfaces, especially the characterization of chemical variegation. If only morphology needs to be characterized, then the problem can be solved by both contact and noncontact techniques. The chemical contrast, especially if both components are organic, may, however, be insufficient to yield a clear distinction between the different components. A practical approach to overcome this problem is selective post-fabrication processing that only affects one of the components.[13]

Morphology

Contact techniques are based on displacing a stylus over the surface. The vertical motions (deflexions from a mean) of the stylus are considered to more or less faithfully mimic the surface topography, which is recorded through a position transducer attached to the stylus. Differences in the realization of the technique are mainly due to the dimensions of the stylus. Of particular interest for the characterization of nanotexture are the SPMs, the first of which was the scanning tunnelling microscope (STM) [56], which have already been mentioned at the beginning of the section "How to generate nanoscale texture in materials" in the context of pick and place fabrication. These instruments are by now too well known to require a detailed description here. An important consideration is that for the finest nanotexture, such as that mimicking the protein surface, the features are smaller than 30–40 nm radius of the typical stylus of an SPM. Hence, in the image generated by the microscope, the apparent lateral dimensions of features will be broadened (see, e.g., [57]). If r is the true feature radius, the apparent lateral dimension L of an object imaged by a tip of radius R is given by

$$L = 4(Rr)^{1/2} \tag{16}$$

This problem can to some degree be overcome by independently measuring the precise shape of the tip, e.g., by using a scanning electron microscope (SEM), and then processing the deflexion profiles recorded using SPM in order to deconvolute the influence of tip shape—this is the exact analogy of the modulation transfer function (MTF) approach used in optical image processing. Alternatively, finer styli (tips) can be used, for example, made by controlled etching of standard tips. These ultrafine tips are,

[13]This principle is applicable more widely than just to the imaging of complex surfaces. For example, iron is a catalyst for CNT growth using (plasma-enhanced) chemical vapor deposition [55], and hence if there is a heterogeneous deposit (islands) of Fe on the surface, each island will serve as an initiator of columnar CNT formation.

however, very fragile and hence easily broken during scanning. CNTs, being extremely thin and rigid, offer a promising alternative to etched tips provided a convenient way of manipulating and attaching them to the microscope cantilever, and possibly replacing them in situ when broken or contaminated, can be found.

A useful extension to the original SPM concept is scanning ion current microscopy (SICM) [58], in which the surface to be characterized is immersed in electrolyte containing a counterelectrode, and the scanning probe is a miniature working electrode inside a very fine glass capillary. The closer the end of the capillary is to the surface, the smaller the ion current, which can, therefore, be used to generate a map of the topography. This method is particularly useful for mechanically imaging ultrafragile samples, such as a living cell, since the capillary never comes into actual content with the surface.

Noncontact methods are based on optics.[14] Optical profilers are analogous to the mechanical stylus instruments but use focused beams to detect the location of the surface. They are, therefore, unlikely to have the resolution required to characterize nanotexture. Light-scattering techniques are in principle more useful, especially for characterizing statistical (ir)regularity. Conventional scattering techniques include specular reflexion, total integrated scattering, and angle-resolved scattering; the newer speckle techniques (speckle contrast, speckle pattern illumination, and angular- or wavelength-dependent speckle correlation [60]) are of particular interest. In the speckle pattern illumination method [61], based on doubly scattered coherent light, the (specularly reflecting) surface is illuminated with a monochromatic speckle pattern, whose phase distribution is then modulated by the rough surface. In polychromatic speckle autocorrelation [62], the (diffusely scattering) surface is illuminated with a collimated, partially coherent (i.e., polychromatic) light beam, either discrete (produced by a combination of laser diodes) or continuous (produced by superbright light-emitting diodes, for example).

Imaging techniques are useful provided the wavelength of the radiation used to generate the image is sufficiently small. This essentially means using energetic electrons; modern high-resolution scanning electron microscopy is able to resolve nanoscale features, provided they are able to conduct the impinging electrons away (which often requires samples to be precoated with a thin metallic film, which is liable to obscure the finest features).

Chemistry

Mapping variegated chemical functionality on the nanoscale is a more difficult problem than mapping topography, and one on which much less research effort has been devoted.

The main family of classical surface chemical analytical methods involve firing one kind of photon (one electron) at the sample and observing the energy of the photons (or electrons) whose emission is thereby triggered.

In Auger electron spectroscopy (AES), an incident electron beam ejects an electron from a core level; the resulting vacancy is unstable and is filled by an electron from a high level, releasing energy that is either transferred to another (Auger) electron (from a yet higher level), or emitted as an X-ray photon. The measurement of the spectrum of the Auger electrons is called AES. In energy-dispersive X-ray spectroscopy (EDS, EDX) it is the X-ray photons whose spectrum is measured. Both these techniques are capable of good lateral resolution (within the nanoscale), because the incident electron beam can be finely focused. EDS is typically carried out within a scanning electron microscope

[14]An important addition to the SPM family is the scanning near-field optical microscope (SNOM), also known as the near-field scanning optical microscope (NSOM). The scanning arrangements remain the same, but now an optical fiber brings light very close to the surface. Transmission, reflexion, and fluorescence can all be measured. The obtainable resolution is below the diffraction limit applicable to far-field optics. A related technique is thermal radiation scanning tunnelling microscopy (TRSTM) [59]. It crosses the boundary from contact to noncontact techniques and has more in common with SNOM than STM.

equipped with a suitable X-ray detector. It yields quantitative elemental abundances with an accuracy of around 1 atom %.

AES, on the other hand, can additionally identify the chemical state of the element. All these techniques yield an average composition within a certain depth from the surface of the sample, which is a complicated function of the scattering of the incident and emergent radiations. Typically, AES samples only the first few nanometers from the surface, whereas EDS averages over a somewhat greater depth, which might be as much as 1 μm.

Techniques such as X-ray fluorescence and X-ray photoelectron spectroscopy, in which the incident photon is an X-ray, have insufficient lateral resolution to be useful for mapping nanotexture.

A different kind of technique is secondary ion mass spectrometry (SIMS), in which a beam of energetic ions (typically, gallium or oxygen) focused on the sample knocks out ions; these ions are detected in a mass spectrometer. Recent advances in ion beam technology have resulted in the introduction of nanoSIMS, with a lateral resolution of a few tens of nanometers. The relationship between the detected ion abundances and the original sample composition strongly depends on the overall constitution of the sample, and hence quantification is usually a difficult challenge. One advantage of SIMS is that the incident ion beam can be used to systematically etch away the sample, allowing the depth profile of the chemical composition to be obtained.

As described in the previous subsection, the metrology of topography has benefited immensely from the development of SPMs, which have largely solved the problem (although there is evidently still room for refinement of the technology). SPM can also be used to yield chemical information about the sample surface. This involves careful measurement of the force-distance characteristics, as the tip is made to approach, and is then retracted from, a particular point on the surface. SPM tips made from different materials can be chosen in order to investigate the combined effects of interfacial forces and surface topography. Lateral resolution is limited by the tip radius. If a rather stiff cantilever is used, its motion will tend to follow the topography of the Born repulsion. A more flexible cantilever will be sensitive to the longer-range, but weaker, electron donor–acceptor and electrostatic interactions [63], which depend upon the chemical composition of the sample at the point being measured.

Contrast enhancement

When attempting to map chemical variegation, it may often be that the contrast between regions of differing chemical functionalities is too low. This is especially likely to be the case when the variegation resides in differing organic functionalities.

In this case, a useful technique may be to allow high contrast objects smaller than the smallest feature size to selectively bind to one functionality. Now that a plethora of very small nanoparticles is available commercially, and others can be chemically synthesized by well-established methods (see, e.g., [33]), this method has become very useful and practicable. Examples of the decoration of block copolymer films are given in refs. [64,65]. Using fairly extensive tabulations of single-substance surface energies, the adhesive force between two substances in the presence and absence of a fluid (in which the nanoparticles will usually be suspended) can be readily estimated (e.g., [63]).

Relationship between morphology and chemistry

Morphology and chemistry are not independent at the nanoscale. Depending on how it is cut, the chemistry of the planar face of a crystal of a binary compound can vary dramatically. "Roughness" or texture at the nanoscale is actually constituted from an intricate array of different crystal facets. The resulting effect depends on the characteristic length scale of the phenomenon being investigated. Living cells, for example, are known to be highly sensitive to the crystallographic orientation of a substratum. This has been demonstrated by cell growth experiments on single crystals: epithelial cells attached themselves and spread only on the (011) faces of calcium carbonate tetrahydrate and not on the (101)

faces, within tens of minutes following initial contact, but after 72 h all cells on the (011) faces were dead, but well-spread and living on the (101) faces [66]. These two faces mainly differ in the surface distribution of the lattice water molecules, but the experiments were of course carried out in the presence of an aqueous cell culture medium. One must also bear in mind that most cells are actively secreting extracellular matrix proteins when in contact with a substratum, which are then interposed to form a layer between the cell and the original substratum material.

ANALYSIS OF TEXTURE

An exhaustive description of a nanotextured surface, in the form of a complete list of the atomic coordinates of each element, would be impracticably cumbersome. Even if nanometrology can, either now or in the future, yield such information, in needs to be interpreted in order to determine the laws governing the effects of nanotexture on the response of, for example, living cells growing on it.

A standard surface analytical technique such as X-ray fluorescence will yield the overall atomic composition. The techniques discussed in the section "Visualizing and converting nanotexture" are aimed at mapping out the chemical and topographical variegation to as fine a resolution as that of any variegation that may be present. Raster techniques such as the SPMs can identify variegation pixel by pixel and produce a one-dimensional string of information a priori suitable for analyzing according to the methods suggested in the section "One-dimensional texture".[15] The main task is to determine the presence of compositional and/or topographical correlations within the plane of the surface. This can be quantified by estimating the algorithmic information content (AIC, also called algorithmic or Kolmogorov complexity [4,5]), which is essentially a formalization of the notion of estimating the complexity of an object from the length of a description of it. The first task is to encode the measured variegation in some standard form. The choice of rules used to accomplish the encoding will depend on the particular problem at hand. For the one-dimensional nucleic acid textures referred to in the section "One-dimensional texture", encoding purines as 1 and pyrimidines as 0 may be sufficient, for example. The formal definition of the AIC of a symbolic string S (encoding the object being described) is "the length of the smallest (shortest) program P that will cause the standard universal computer (a Turing machine T) to print out the symbolic string and then halt". Symbolically (but only exact for infinite strings), denoting the AIC by K,

$$K(s) = \min\{|\mathrm{P}| : s = C_{\mathrm{T}}(\mathrm{P})\} \tag{17}$$

where $|\mathrm{P}|$ is the length of the program (in bits) and C_{T} is the result of running the program on a Turing machine. Any regularity present within the string will enable the description to be shortened. The determination of AIC is therefore essentially one of pattern recognition, which works by comparing the unknown object with known prototypes (there is no algorithm for discovering patterns de novo, although clustering according to the distances between features (cf. footnote 1) may help). The maximum value of the AIC (the unconditional complexity) is equal to the length of the string in the absence of any internal correlations, that is, considering the string as random, viz.,

$$K_{\max} = |s| \tag{18}$$

Any regularities, i.e., constraints in the choice of successive symbols, will diminish the value of K from $K_{\max}$.

The concept of effective complexity (EC) [67] was introduced in an effort to overcome the problem of AIC increasing monotonically with increasing randomness. EC is defined as the length of a con-

[15]The to and fro motion of the scanning probe imposes a certain kind of correlation on the symbolic sequence if there are two-dimensional features present (i.e., thicker than a single scanning line).

cise description (which can be computed in the same way as the AIC) of the set of regularities of the description. A very regular symbolic sequence will have only a small number of different regularities, and therefore a short description of them; a random sequence will have no regularities, and therefore an even shorter description. There will be some intermediate descriptions with many different regularities, which will yield a large EC. Essentially,

$$\mathrm{EC} = \mathrm{AIC} - \mathrm{RIC} \tag{19}$$

where RIC is the random information content. In a certain sense, EC is actually a measure of our knowledge about the object being described, for it quantifies the extent to which the object is regular (nonrandom), and hence predictable. It presents the same technical difficulty as AIC: that of finding the regularities, both in compiling an initial list of them, and then in finding the regularities of the regularities.

Lacunarity

Whereas AIC and EC can be straightforwardly applied to linear texture, it is not generally obvious how the two-dimensional pattern should be encoded. Of course, it could be mapped in raster fashion (as is actually done in SPM and SEM), and patterns extending over many lines should appear as regularities.

Another approach to capturing information about the spatial correlations of arbitrarily heterogeneous real surfaces is to extend the fractional dimension or fractal representation of roughness to encompass the quantification of voids in rough objects (the lacunarity Λ). Consider an image constructed from binary (black or white, corresponding to values of 0 and 1) pixels, and let the numbers of boxes of side r containing s white pixels have the distribution $n(s, r)$. $\Lambda(r)$ is defined as

$$\Lambda(r) = M_2/M_1^2 \tag{20}$$

where M_1 and M_2 are the first and second moments of the distribution,

$$M_1(r) = \sum_{s=1}^{r^2} s(r)\, n(s,r) / N(r) = \langle s(r) \rangle \tag{21}$$

and

$$M_2(r) = \sum_{s=1}^{r^2} s^2(r)\, n(s,r) / N(r) = \sigma_s^2(r) + \langle s \rangle^2(r) \tag{22}$$

where $\langle s \rangle$ and σ_s^2 are, respectively, the mean and variance of the distribution; and the total number $N(r) = (M - r + 1)^2$ for a square pattern of size M of boxes of size r (i.e., a type of variance-to-mean ratio). The lacunarity can be thought of as the deviation of a fractal from translational invariance [68], or a scale-dependent measure of heterogeneity (i.e., "texture") of objects in general [69]. Its lowest possible value is 1, corresponding to a translationally invariant pattern (including the special case $\Lambda(M) = 1$). Practical approaches to determining the lacunarity are described in ref. [70]. The typical output is the lacunarity plot [i.e., a log–log plot of the function $\Lambda(r)$]. Comparison of the lacunarity plots of artificially generated patterns with the experimental lacunarity may be used to analyze the texture of the sample.

CONCLUSIONS

Nanotexture is a crucial aspect of molecular recognition. Its careful study is of particular value in understanding how to design artificial surfaces for interfacing with living matter, or biological macromolecules.

The three principal approaches to generating nanotexture artificially over sufficient area to be practically useful at the macroscale are: (1) the assembly of mixtures of different nanoparticles; (2) the mixing of incompatible polymers with prevention of microscopic phase separation; and (3) the felting of mixtures of different fibers.

The metrology of nanotexture is strongly based around SPM, but the mapping of chemical nanotexture is still difficult, and further significant progress is to be anticipated.

After the metrology has reduced the nanotexture to a symbolic array, a number of formal information-theoretic techniques exist to parametrize texture. These are best understood and easiest to apply in the case of one-dimensional symbolic strings, but encouraging progress is being made in treating two-dimensional pattern.

REFERENCES

1. W. Dowhan. *Annu. Rev. Biochem.* **66**, 199 (1997).
2. C. Calonder, J. Talbot, J. J. Ramsden. *J. Phys. Chem. B* **105**, 725 (2001).
3. G. Crabbe. *Universal Technological Dictionary*, Baldwin, Cradock and Joy, London (1823).
4. J. J. Ramsden. In *Complexity and Security*, J. J. Ramsden, P. J. Kervalishvili (Eds.), pp. 55–70, IOS Press, Amsterdam (2008).
5. J. J. Ramsden. In *Complexity and Security*, J. J. Ramsden, P. J. Kervalishvili (Eds.), pp. 93–102, IOS Press, Amsterdam (2008).
6. B. Schwikowski, P. Uetz, S. Fields. *Nat. Biotechnol.* **18**, 1257 (2000).
7. U. Stelzl, U. Worm, M. Lalowski, C. Haenig, F. H. Brembeck, H. Goehler, M. Stroedicke, M. Zenkner, A. Schoenherr, S. Koeppen, J. Timm, S. Mintzlaff, C. Abraham, N. Bock, S. Kietzmann, A. Goedde, E. Toksöz, A. Droege, S. Krobitsch, B. Korn, W. Birchmeier, H. Lehrach, E. E. Wanker. *Cell* **122**, 957 (2005).
8. A. Fernández, R. Scott. *Biophys. J.* **85**, 1914 (2003).
9. S. Damjanovich, R. Gaspar, C. Pieri. *Q. Rev. Biophys.* **30**, 67 (1997).
10. Terminology for the Bio-Nano Interface (Publicly Available Specification, PAS132:2007). British Standards Institute, London (2007).
11. J. Gorelik, A. I. Shevchuk, G. I. Frolenkov, I. A. Diakonov, M. J. Lab, C. J. Kros, G. P. Richardson, I. Vodyanoy, C. R. W. Edwards, D. Klenerman, Yu. E. Korchev. *Proc. Natl Acad. Sci. USA* **100**, 5819 (1981).
12. W. Feller. *An Introduction to Probability Theory and its Applications*, 3rd ed., Vol. 1, John Wiley, New York (1967).
13. A. M. Mood. *Ann. Math. Statist.* **11**, 367 (1940).
14. J. J. Ramsden. *Bioinformatics: An Introduction*, Kluwer, Dordrecht (2004).
15. A. A. Markov. *Izv. Imp. Akad. Nauk. Ser.* **6**, 153 (1913) (in Russian).
16. K. E. Drexler. *Proc. Natl. Acad. Sci. USA* **78**, 5275 (1981).
17. E. K. Schweizer, D. M. Eigler. *Nature (London)* **344**, 524 (1990).
18. N. Oyabu, O. Custance, I. Yi, Y. Sugawara, S. Morita. *Phys. Rev. Lett*. **90**, 176102 (2003).
19. N. Oyabu, P. Pou, Y. Sugimoto, P. Jelinek, M. Abe, S. Morita, R. Perez, O. Custance. *Phys. Rev. Lett*. **96**, 106101 (2006).
20. S. de Haan. *Nanotechnol. Perceptions* **2**, 267 (2006).
21. K. E. Drexler. *Nanosystems: Molecular Machinery, Manufacturing, and Computation*, John Wiley, New York (1992).
22. K.-B. Lee, J.-H. Lim, C. A. Mirkin. *J. Am. Chem. Soc*. **125**, 5588 (2003).
23. H. Zhang, K.-B. Lee, Z. Li, C. A. Mirkin. *Nanotechnology* **14**, 1113 (2003).
24. A. G. Mamalis, A. Markopoulos, D. E. Manolakos. *Nanotechnol. Perceptions* **1**, 31 (2005).
25. J. J. Ramsden, D. M. Allen, D. J. Stephenson, J. R. Alcock, G. N. Peggs, G. Fuller, G. Goch. *Ann. CIRP* **5612**, 687 (2007).

26. P. O. Luthi, A. Preiss, B. Chopard, J. J. Ramsden. *Physica D* **118**, 151 (1998).
27. S. F. Edwards, R. D. S. Oakeshott. *Physica A* 157, 1080 (1989).
28. A. Naydenov, P. A. Pincus, S. A. Safran. *Langmuir* **23**, 12016 (2007).
29. J. J. Ramsden, M. Máté. *J. Chem. Soc., Faraday Trans.* **94**, 783 (1998).
30. G. Tolnai, A. Agod, M. Kabai-Faix, A. L. Kovács, J. J. Ramsden, Z. Hórvölgyi. *J. Phys. Chem. B* **107**, 11109 (2003).
31. Y. Zhang, V. T. Milam, D. J. Graves, D. A. Hammer. *Biophys. J.* **90**, 4128 (2006).
32. S. Alexandre, C. Lafontaine, J.-M. Valleton. *J. Biol. Phys. Chem.* **1**, 21 (2001).
33. J. J. Ramsden. *Surf. Sci.* **156**, 1027 (1985).
34. J. J. Ramsden. *Proc. R. Soc. London, Ser. A* **413**, 407 (1987).
35. W. Cooper, W. Nuttall. *J. Agric. Sci.* **7**, 219 (1915).
36. P. G. de Gennes. *Rev. Mod. Phys.* **57**, 827 (1985).
37. S. Ortmann, A. Savan, Y. Gerbig, H. Haefke. *Wear* **254**, 1099 (2003).
38. E. Mirica, G. Kowach, H. Du. *Cryst. Growth Des.* **4**, 157 (2004).
39. S. C. G. Leeuwenburgh, M. C. Heine, J. C. G. Wolke, S. E. Pratsinis, J. Schoonman, J. A. Jansen. *Thin Solid Films* **503**, 69 (2006).
40. C. M. Dekeyser, S. Biltresse, J. Marchand-Brynaert, P. G. Rouxhet, Ch. C. Dupont-Gillain. *Polymer* **45**, 2211 (20044).
41. D. J. Meier. *J. Polym. Sci.* C **26**, 81 (1969).
42. F. S. Bates, G. H. Fredrickson. *Annu. Rev. Phys. Chem.* **41**, 525 (1990).
43. F. S. Bates, G. H. Fredrickson. *Physics Today* **52**, 32 (1999).
44. G. Krausch, R. Magerle. *Adv. Mater.* **14**, 1579 (2002).
45. J. P. Spatz, P. Eibeck, S. Mössmer, M. Möller, E. Yu. Kramarenko, P. G. Khalatur, I. I. Potemkin, A. R. Khokhlov, R. G. Winkler, P. Reineker. *Macromolecules* **33**, 150 (2000).
46. T. Xu, H.-C. Kim, J. DeRouchey, C. Seney, C. Levesque, P. Martin, C. M. Stafford, T. P. Russell, *Polymer* **42**, 9091 (2001).
47. T. Hashimoto, H. Tanaka, H. Hasegawa. *Macromolecules* **23**, 4378 (1990).
48. J. J. Ramsden. *Nanotechnology in Paper Production*, Pira International, Leatherhead (2005).
49. R. L. D. Whitby, T. Fukuda, T. Maekawa, S. L. James, S. V. Mikhalovsky. *Carbon* **46**, 949 (2008).
50. L. J. Hall, V. R. Coluci, D. S. Galvão, M. E. Kozlov, M. Zhang, S. O. Dantas, R. H. Baughman. *Science* **320**, 504 (2008).
51. J. McColl, G. E. Yakubov, J. J. Ramsden. *Langmuir* **23**, 7096 (2007).
52. J. J. Ramsden. *Biopolymers* **33**, 475 (1993).
53. S. J. Eichhorn, W. W. Sampson. *J. R. Soc. Interface* **2**, 309 (2005).
54. W. W. Sampson. *Filtration* **7**, 251 (2007).
55. B. O. Boscovic. *Nanotechnol. Perceptions* **3**, 141 (2007).
56. G. Binnig, H. Rohrer. *Helv. Phys. Acta* **55**, 726 (1982).
57. U. D. Schwarz, H. Haefke, P. Reimann, H. Guentherodt. *J. Microscopy* **173**, 183 (1994).
58. A. Shevchuk, J. Gorelik, S. Harding, M. Lab, D. Klenerman, Y. E. Korchev. *Biophys. J.* **81**, 1759 (2001).
59. Y. de Wilde, F. Formanek, R. Carminati, B. Gralak, P. A. Lemoine, K. Joulain, J. P. Mulet, Y. Chen, J. J. Greffet. *Nature (London)* **444**, 740 (2006).
60. P. Lehmann, G. Goch. *Ann. CIRP* **49**, 419 (2000).
61. P. Lehmann. *Appl. Opt.* **38**, 1144 (1999).
62. P. Lehmann, S. Patzelt, A. Schöne. *Appl. Opt.* **36**, 2188 (1997).
63. M. G. Cacace, E. M. Landau, J. J. Ramsden. *Q. Rev. Biophys*. **30**, 241 (1997).
64. T. L. Morkved, P. Wiltzius, H. M. Jaeger, D. G. Grier, T. A. Witten. *Appl. Phys. Lett.* **64**, 422 (1994).
65. W. A. Lopes, H. M. Jaeger. *Nature (London)* **414**, 735 (2001).
66. D. Hanein, H Sabanay, L. Addadi, B. Geiger. *J. Cell Sci.* **104**, 27 (1993).

67. M. Gell-Mann, S. Lloyd. *Complexity* **2**, 44 (1996).
68. Y. Gefen, Y. Meir, A. Aharony. *Phys. Rev. Lett.* **50**, 145 (1983).
69. C. Allain, M. Cloitre. *Phys. Rev. A* **44**, 3552 (1991).
70. J. J. Ramsden. *Biomedical Surfaces*, pp. 74–77, Artech House, Norwood, MA (2008).